

Measurement of the $e^+e^- \rightarrow \eta\pi^+\pi^-$ cross section with the SND detector at the VEPP-2000 collider

M. N. Achasov,^{1,2} A. Yu. Barnyakov,^{1,2} K. I. Beloborodov,^{1,2} A. V. Berdyugin,^{1,2} D. E. Berkaev,^{1,2}
A. G. Bogdanchikov,¹ A. A. Botov,¹ T. V. Dimova,^{1,2} V. P. Druzhinin,^{1,2,*} V. B. Golubev,^{1,2}
L. V. Kardapoltsev,^{1,2} A. G. Kharlamov,^{1,2} I. A. Koop,^{1,2,3} A. A. Korol,^{1,2} D. P. Kovrizhin,¹
S. V. Koshuba,¹ A. S. Kupich,^{1,2} A. P. Lysenko,¹ K. A. Martin,¹ N. A. Melnikova,^{1,2} N. Yu. Muchnoi,^{1,2}
A. E. Obrazovsky,¹ E. V. Pakhtusova,¹ E. A. Perevedentsev,^{1,2} K. V. Pugachev,^{1,2} E. V. Rogozina,^{1,2}
S. I. Serednyakov,^{1,2} Z. K. Silagadze,^{1,2} Yu. M. Shatunov,^{1,2} P. Yu. Shatunov,^{1,2} D. A. Shtol,¹
I. K. Surin,¹ Yu. A. Tikhonov,^{1,2} Yu. V. Usov,¹ A. V. Vasiljev,^{1,2} and I. M. Zemlyansky^{1,2}

¹*Budker Institute of Nuclear Physics, SB RAS, Novosibirsk, 630090, Russia*

²*Novosibirsk State University, Novosibirsk, 630090, Russia*

³*Novosibirsk State Technical University, Novosibirsk, 630092, Russia*

The $e^+e^- \rightarrow \eta\pi^+\pi^-$ cross section is measured at the SND detector in the η decay mode $\eta \rightarrow 3\pi^0$. The analysis is based on the data sample with an integrated luminosity of 32.7 pb^{-1} collected at the VEPP-2000 e^+e^- collider in the center-of-mass energy range $\sqrt{s} = 1.075 - 2.000 \text{ GeV}$. The data obtained in the $\eta \rightarrow 3\pi^0$ decay mode are found to be in agreement with the previous SND measurements in the $\eta \rightarrow \gamma\gamma$ mode. Therefore the measurements in the two modes are combined.

I. INTRODUCTION

In this paper we continue the study of the process $e^+e^- \rightarrow \eta\pi^+\pi^-$ with the SND detector at the VEPP-2000 e^+e^- collider begun in Ref. [1]. This isovector process proceeding mainly via the $\rho\eta$ intermediate state [1] is important for spectroscopy of the excited ρ -like states, $\rho(1450)$ and $\rho(1700)$, and gives a sizable contribution into the total hadronic cross section at the center-of-mass (c.m.) energy region $\sqrt{s} = 1.4 - 1.8 \text{ GeV}$. The $e^+e^- \rightarrow \eta\pi^+\pi^-$ cross-section data can be used to predict the hadronic spectral function in the $\tau^- \rightarrow \eta\pi^- \pi^0 \nu_\tau$ decay and thus to test the hypothesis of conservation of vector current.

Previously the $e^+e^- \rightarrow \eta\pi^+\pi^-$ process was studied in several experiments [1–6]. The most complete and accurate data were obtained by BABAR [5] and SND at VEPP-2000 [1]. In Ref. [1], the η -meson was reconstructed via its decay mode $\eta \rightarrow 2\gamma$. The cross section was measured in the energy region from 1.22 to 2.00 GeV. Large background from the $e^+e^- \rightarrow \pi^+\pi^-\pi^0\pi^0$ and other hadronic processes didn't allow to perform measurement with comparable accuracy at lower energies. In this work, we use the decay mode $\eta \rightarrow 3\pi^0$, in which the detection efficiency is lower, but the signal-to-background ratio is better, to improve measurement sensitivity below 1.2 GeV.

II. DETECTOR AND EXPERIMENT

SND is a nonmagnetic detector [7] collecting data at the VEPP-2000 e^+e^- collider [8] in the energy range $\sqrt{s} = 0.3 - 2.0 \text{ GeV}$. The direction and vertex position of charged particles are measured by a nine-layer cylindrical drift chamber. Charged particle identification is based on dE/dx measurements in the drift chamber and information from the system of threshold aerogel Cherenkov counters. The photon energies and directions are measured in a three-layer spherical electromagnetic calorimeter based on NaI(Tl) crystals. The calorimeter covers a solid angle of about 95% of 4π . Its energy resolution for photons is $\sigma_{E_\gamma}/E_\gamma = 4.2\%/\sqrt[4]{E_\gamma(\text{GeV})}$, and the angular resolution is about 1.5° . Outside the calorimeter, a muon detector consisting of proportional tubes and scintillation counters is placed.

This work is based on a data sample with an integrated luminosity of 32.7 pb^{-1} collected in 2011–2012 in the c.m. energy range $\sqrt{s} = 1.075 - 2 \text{ GeV}$. The energy range was scanned several times with a step of 25 MeV. During the experiment, the beam energy was determined using measurements of the magnetic field in the collider bending magnets. To fix the absolute energy scale, the $\phi(1020)$ resonance mass measurement was performed. In 2012 the beam energy was measured in several energy points near 2 GeV by the back-scattering-laser-light system [9, 10]. The absolute energy measurements were used for calibration of the momentum measurement in the CMD-3 detector,

*e-mail:druzhinin@inp.nsk.su

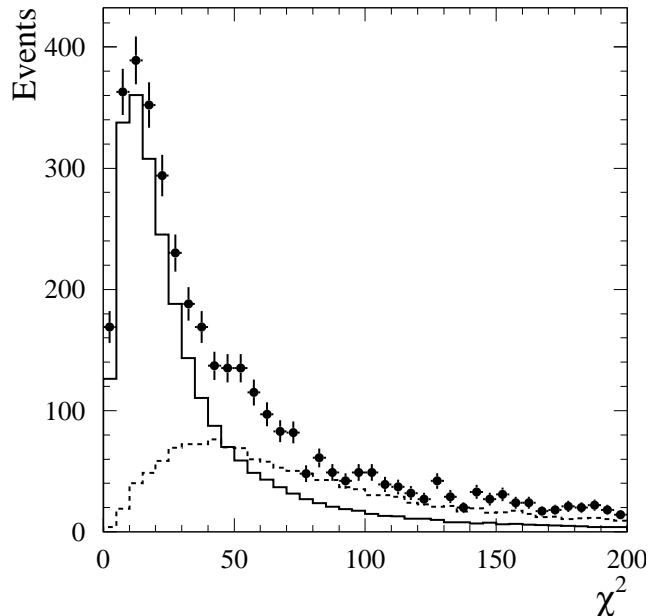


Figure 1: The $\chi_{5\pi}^2$ distribution for data events with $1.4 \leq \sqrt{s} \leq 1.8$ GeV selected with the additional condition $500 < M_{3\pi^0} < 600$ MeV/ c^2 (points with error bars) in comparison with the simulated distributions for signal (solid histogram) and background $e^+e^- \rightarrow \pi^+\pi^-\pi^0\pi^0$ events (dashed histogram).

which collected data at VEPP-2000 simultaneously with SND. The absolute c.m. energies for all scan points were then determined using average momentum in Bhabha and $e^+e^- \rightarrow p\bar{p}$ events with accuracy of 2 – 6 MeV [11].

Simulation of the signal processes is done with the Monte Carlo (MC) event generator based on formulas from Ref. [12] and uses the model of the $\eta\rho(770)$ intermediate state. The generator takes into account radiative corrections to the initial particles calculated according to Ref. [13]. The angular distribution of additional photons radiated by the initial particles is simulated according to Ref. [14]. The $e^+e^- \rightarrow \eta\pi^+\pi^-$ cross-section energy dependence needed for radiative-correction calculation is taken from Ref. [1]. Interactions of the generated particles with the detector material are simulated using GEANT4 package [15]. The simulation takes into account variation of experimental conditions during data taking, in particular, dead detector channels and beam-induced background. The beam background leads to appearance of spurious photons and charged particles in detected events. To take this effect into account, special background events recorded during data taking with a random trigger are used, which are superimposed on simulated events.

The process of Bhabha scattering $e^+e^- \rightarrow e^+e^-$ is used for luminosity measurement. Accuracy of the luminosity measurement is estimated to be 2% [1].

III. EVENT SELECTION

In this analysis the η meson is reconstructed via its decay $\eta \rightarrow 3\pi^0$. Therefore, we select events with two charged particles originated from the interaction region and at least six photons.

For selected events the vertex fit is performed using parameters of two charged tracks. The χ^2 of the vertex fit (χ_{vertex}^2) is required to be less than 200. The found vertex is used to refine the parameters of charged particles and photons. Then the kinematic fit to the $e^+e^- \rightarrow \pi^+\pi^-3\pi^0$ hypothesis is performed with the requirement of energy and momentum balance and the π^0 mass constraints. The π^0 candidate is a two photon pair with invariant mass in the range 90 – 200 MeV/ c^2 . The quality of the kinematic fit is characterized by the parameter $\chi_{5\pi}^2$, which is required to be less than 45. If more than one photon combination satisfies this condition, the combination with the smallest $\chi_{5\pi}^2$ value is chosen. Photon parameters corrected during the kinematic fit are used to calculate the invariant mass of the three π^0 candidates ($M_{3\pi^0}$).

To suppress background from the process $e^+e^- \rightarrow \pi^+\pi^-\pi^0\pi^0$, the kinematic fit to the $e^+e^- \rightarrow \pi^+\pi^-\pi^0\pi^0$ hypothesis is performed, and the condition $\chi_{4\pi}^2 > 20$ is applied.

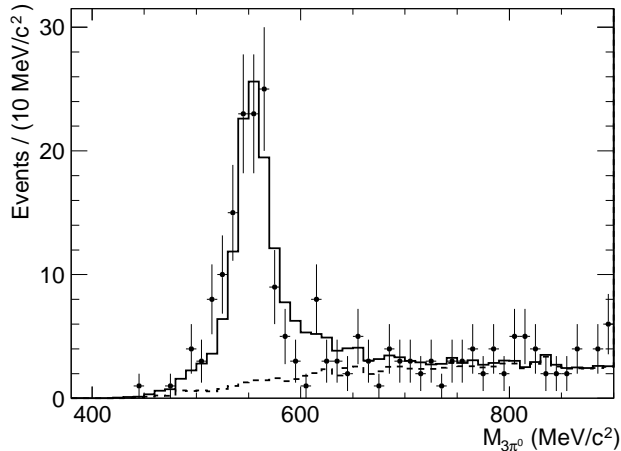


Figure 2: The $M_{3\pi^0}$ spectrum for selected data events with $\sqrt{s} = 1.55$ GeV (points with error bars). The solid histogram is the results of the fit by a sum of signal and background distributions. The dashed histogram represents the fitted background spectrum.

The $\chi^2_{5\pi}$ distribution for data events from the energy region $1.4 \leq \sqrt{s} \leq 1.8$ GeV selected with the additional condition $500 < M_{3\pi^0} < 600$ MeV/ c^2 is shown in Fig. 1 in comparison with the simulated distributions for signal and background $e^+e^- \rightarrow \pi^+\pi^-\pi^0\pi^0$ events.

IV. DETERMINATION OF THE NUMBER OF SIGNAL EVENTS

The $M_{3\pi^0}$ spectrum for selected data events with $\sqrt{s} = 1.55$ GeV is shown in Fig. 2. The spectrum is fitted with a sum of signal and background distributions. The signal distribution is described by a sum of three Gaussian functions with parameters determined from the fit to the $M_{3\pi^0}$ distribution for simulated signal events. To account for a possible inaccuracy of the signal simulation, two parameters are introduced: mass shift ΔM and a width correction $\Delta\sigma^2$. The latter parameter is added to all Gaussian sigmas squared ($\sigma^2 = \sigma_{MC}^2 + \Delta\sigma^2$). These parameters are determined from the fit to the spectrum for data events from the energy interval near the maximum of the $e^+e^- \rightarrow \eta\pi^+\pi^-$ cross section ($\sqrt{s} = 1.45 - 1.60$ GeV) and found to be $\Delta M = -(3.1 \pm 0.9)$ MeV/ c^2 and $\Delta\sigma^2 = -(24 \pm 19)$ MeV $^2/c^4$ for 2011 data set, and $-(3.4 \pm 1.5)$ MeV/ c^2 and 56 ± 47 MeV $^2/c^4$ for 2012 data set.

The background distribution is obtained using simulation of the processes $e^+e^- \rightarrow \pi^+\pi^-\pi^0\pi^0$, $e^+e^- \rightarrow \omega\pi^0\pi^0$, and $e^+e^- \rightarrow \pi^+\pi^-\pi^0\eta$. To calculate expected numbers of background events we use existing data on the cross sections, in particular, the preliminary SND measurement [16] for the $e^+e^- \rightarrow \pi^+\pi^-\pi^0\eta$ cross section. A possible inaccuracy of background calculation is taken into account by introducing a scale factor α_{bkg} . For energies below 1.6 GeV, the value of α_{bkg} found in the fit is consistent with unity. At higher energies, there is significant background contribution from other hadronic processes, e.g., $e^+e^- \rightarrow \pi^+\pi^-\pi^0\pi^0\eta$, or $e^+e^- \rightarrow \pi^+\pi^-4\pi^0$, cross section for which are unknown. In this region, the background is described by a function based on the ARGUS distribution [17]. It has been tested that this function describes well the shape of the $M_{3\pi^0}$ spectra for all background processes mentioned above. The example of the fit with ARGUS background is shown in Fig. 3.

To study the systematic uncertainty associated with the description of background shape, the $M_{3\pi^0}$ spectrum for the energy region $\sqrt{s} = 1.45 - 1.60$ GeV is fitted with the function based on the ARGUS distribution. The difference between numbers of signal events obtained with this fit and the fit with the simulated background shape is found to be 6%. This number is taken as an estimate of the systematic uncertainty on the number of fitted signal events.

The numbers of fitted $e^+e^- \rightarrow \eta\pi^+\pi^-$ events for different energy points are listed in Table II.

V. DETECTION EFFICIENCY

The detection efficiency is determined using MC simulation and then corrected for data-MC simulation difference in detector response: $\varepsilon = \varepsilon_{MC}/(1-\Delta)$. The correction for a specific selection criterion is calculated as $\Delta = \frac{(N^*/N)_{\text{data}}}{(N^*/N)_{\text{MC}}} - 1$, where N and N^* are the numbers of signal events selected with the standard and loosened criterion.

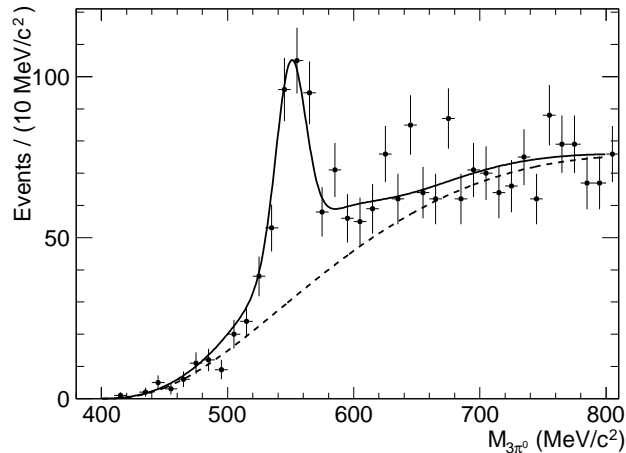


Figure 3: The $M_{3\pi^0}$ spectrum for selected data events with $\sqrt{s} = 1.7 - 2.0$ GeV (points with error bars). The solid curve is the result of the fit by a sum of signal and background distributions. The dashed curve represents the fitted background spectrum.

Table I: Efficiency corrections

Effect	Δ , %
Condition $\chi_{\pi^+\pi^-3\pi^0}^2 < 45$	-1.5 ± 2.7
Condition $\chi_{\text{vertex}}^2 < 200$	0.9 ± 0.4
Track reconstruction	0.3 ± 0.2
Photon conversion	2.0 ± 0.2
Total	1.7 ± 2.8

The efficiency corrections are listed in Table I. To obtain the correction for the condition $\chi_{\pi^+\pi^-3\pi^0}^2 < 45$ we use data from the energy region $\sqrt{s} = 1.425 - 1.68$ GeV and change the boundary of the condition from 45 to 1000. The corrections for the condition $\chi_{\text{vertex}}^2 < 200$ and track-reconstruction inefficiency are taken from Ref. [1]. The data-MC simulation difference in photon conversion in detector material before the tracking system is studied using events of the process $e^+e^- \rightarrow \gamma\gamma$.

The corrected detection efficiency as a function of the c.m. energy is listed in Table II. Nonmonotonic behavior of the efficiency is due to variations of experimental conditions (beam background, dead detector channels, etc.). The efficiency decrease above 1.6 GeV is explained by the decrease of the $e^+e^- \rightarrow \eta\pi^+\pi^-$ cross section in this energy region and increase of the fraction of events with a hard photon radiated from the initial state, which are rejected by the cut $\chi_{\pi^+\pi^-3\pi^0}^2 < 45$.

The model dependence of the detection efficiency originating from the uncertainty of the $e^+e^- \rightarrow \eta\pi^+\pi^-$ cross section used in simulation was studied in Ref. [1]. It was found to be 1.0% at $\sqrt{s} < 1.6$ and 4.2% GeV at higher energies.

VI. THE $e^+e^- \rightarrow \eta\pi^+\pi^-$ BORN CROSS SECTION

The experimental value of the Born cross section for the i th energy point is calculated as follows,

$$\sigma_{\text{B},i} = \frac{N_i}{L_i(1 + \delta_i)\varepsilon_i}, \quad (1)$$

where L_i is the integrated luminosity, N_i is the number of signal events, ε_i is the detection efficiency, and δ_i is the radiative correction. The latter is determined as a result of the fit to data on the visible cross section

$$\sigma_{\text{vis},i} = \frac{N_i}{L_i\varepsilon_i} \quad (2)$$

Table II: The c.m. energy (\sqrt{s}), integrated luminosity (L), number of signal events (N), detection efficiency (ε), radiative-correction factor ($1+\delta$), $e^+e^- \rightarrow \eta\pi^+\pi^-$ Born cross section measured in the $\eta \rightarrow 3\pi^0$ decay mode (σ_B for $\eta \rightarrow 3\pi^0$), and $e^+e^- \rightarrow \eta\pi^+\pi^-$ Born cross section combined with the SND measurement [1] in the $\eta \rightarrow \gamma\gamma$ decay mode (σ_B). The quoted errors are statistical. The systematic uncertainties are discussed in the text. For the combined cross section it is 7% below 1.45 GeV, 6% at $1.45 < \sqrt{s} < 1.6$ GeV, and 8% above 1.6 GeV.

\sqrt{s} (GeV)	L (nb $^{-1}$)	N	ε (%)	$1 + \delta$	σ_B for $\eta \rightarrow 3\pi^0$ (nb)	σ_B (nb)
1.075	541	11 ± 7	6.0	0.874	0.37 ± 0.25	0.37 ± 0.25
1.097	541	3 ± 4	6.1	0.876	0.09 ± 0.15	0.09 ± 0.15
1.124	528	4 ± 6	6.1	0.877	0.13 ± 0.20	0.13 ± 0.20
1.151	472	4 ± 4	5.9	0.877	0.17 ± 0.16	0.17 ± 0.16
1.174	532	2 ± 5	6.0	0.876	0.08 ± 0.19	0.08 ± 0.19
1.196	536	6 ± 4	5.7	0.875	0.21 ± 0.16	0.21 ± 0.16
1.223	553	8 ± 6	5.8	0.873	0.30 ± 0.23	0.33 ± 0.13
1.245	466	3 ± 4	5.8	0.871	0.13 ± 0.18	0.15 ± 0.12
1.275	1225	13 ± 8	6.3	0.867	0.19 ± 0.13	0.33 ± 0.09
1.295	484	12 ± 5	5.5	0.864	0.53 ± 0.23	0.51 ± 0.15
1.323	542	17 ± 6	5.5	0.862	0.67 ± 0.24	0.71 ± 0.16
1.351	1398	64 ± 11	5.5	0.861	0.96 ± 0.17	1.02 ± 0.12
1.374	599	32 ± 8	5.4	0.863	1.17 ± 0.30	1.22 ± 0.19
1.394	643	62 ± 10	5.2	0.865	2.13 ± 0.33	1.86 ± 0.20
1.423	591	50 ± 9	5.4	0.870	1.79 ± 0.32	2.06 ± 0.21
1.438	1442	227 ± 18	5.1	0.873	3.54 ± 0.28	3.03 ± 0.16
1.471	608	92 ± 12	5.3	0.883	3.21 ± 0.42	3.29 ± 0.25
1.494	731	145 ± 14	5.4	0.893	4.10 ± 0.40	3.82 ± 0.24
1.517	1395	302 ± 21	5.5	0.905	4.35 ± 0.30	4.44 ± 0.19
1.543	566	139 ± 14	5.3	0.921	5.07 ± 0.50	4.55 ± 0.28
1.572	436	101 ± 12	5.2	0.943	4.69 ± 0.55	3.94 ± 0.30
1.594	446	78 ± 15	5.2	0.962	3.54 ± 0.70	3.34 ± 0.31
1.623	530	50 ± 13	5.2	0.987	1.85 ± 0.49	3.12 ± 0.28
1.643	490	55 ± 15	5.0	1.004	2.25 ± 0.60	2.45 ± 0.28
1.672	1314	150 ± 22	5.3	1.021	2.09 ± 0.32	2.30 ± 0.16
1.693	472	55 ± 13	4.8	1.022	2.36 ± 0.57	2.67 ± 0.27
1.720	1022	136 ± 17	4.8	1.010	2.75 ± 0.34	2.23 ± 0.17
1.751	1197	152 ± 24	4.8	1.000	2.63 ± 0.41	2.36 ± 0.17
1.774	473	41 ± 11	4.6	1.016	1.84 ± 0.51	1.96 ± 0.25
1.797	1391	113 ± 22	4.8	1.048	1.61 ± 0.33	2.00 ± 0.16
1.826	513	33 ± 10	4.3	1.095	1.38 ± 0.46	1.44 ± 0.22
1.843	1369	77 ± 19	4.4	1.120	1.14 ± 0.32	1.31 ± 0.14
1.873	1556	84 ± 18	4.0	1.164	1.16 ± 0.29	0.97 ± 0.13
1.900	2033	58 ± 21	3.5	1.200	0.69 ± 0.30	0.79 ± 0.10
1.927	1256	37 ± 14	3.7	1.234	0.66 ± 0.31	0.76 ± 0.13
1.947	1312	40 ± 15	3.8	1.260	0.63 ± 0.30	0.71 ± 0.12
1.967	724	25 ± 12	3.6	1.283	0.75 ± 0.47	0.74 ± 0.18
1.984	1125	30 ± 15	3.7	1.304	0.56 ± 0.36	0.74 ± 0.15
2.005	576	14 ± 11	3.2	1.328	0.57 ± 0.60	0.78 ± 0.22

with the function

$$\sigma_{\text{vis}}(s) = \int_0^{z_{\text{max}}} \sigma_B(s(1-z))F(z,s)dz = \sigma_B(s)(1+\delta(s)), \quad (3)$$

where $F(z,s)$ is the function describing the probability of emission of photons with the energy $z\sqrt{s}/2$ by the initial electron and positron [13], $z_{\text{max}} = 1 - (m_\eta + 2m_\pi)^2/s$, and m_η and m_π are the η and π^- masses.

The vector meson dominance (VMD) model with three intermediate isovector states, $\rho(770)$, $\rho(1450)$ and $\rho(1700)$, decaying into $\eta\rho(770)$ [12] is used to describe the Born cross section:

$$\sigma_B(s) = \frac{4\pi\alpha^2}{3s^{3/2}} |F_{\rho\eta\gamma}(s)|^2 P_f(s), \quad (4)$$

where α is the fine structure constant, $F_{\rho\eta\gamma}(s)$ is the transition form factor for the vertex $\gamma^* \rightarrow \rho\eta$, $P_f(s)$ is the

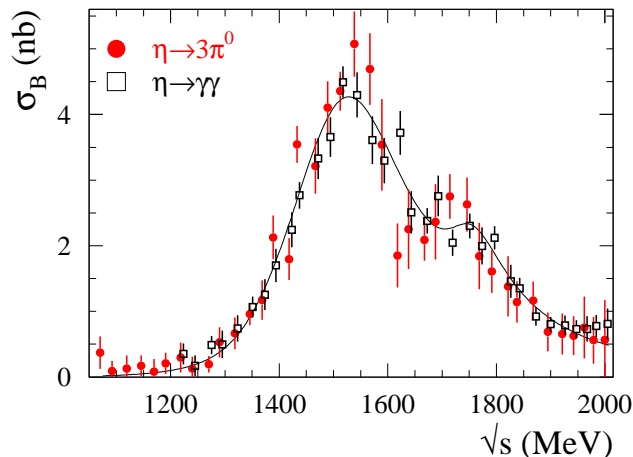


Figure 4: The $e^+e^- \rightarrow \eta\pi^+\pi^-$ Born cross section measured by SND in the $\eta \rightarrow 3\pi^0$ and $\eta \rightarrow \gamma\gamma$ decay modes. The curve is the result of the fit described in text.

function describing the energy dependence of the $\eta\rho(770)$ phase space:

$$\begin{aligned}
 P_f(s) &= \frac{1}{\pi} \int_{4m_\pi^2}^{(\sqrt{s}-m_\eta)^2} \frac{\sqrt{q^2}\Gamma_\rho(q^2)}{(q^2 - m_\rho^2)^2 + q^2\Gamma_\rho^2(q^2)} p^3(q^2) dq^2, \\
 p(q^2) &= \sqrt{\frac{(s - m_\eta^2 - q^2)^2 - 4m_\eta^2 q^2}{4s}}, \\
 \Gamma_\rho(q^2) &= \Gamma_\rho \frac{m_\rho^2}{q^2} \left(\frac{q^2 - 4m_\pi^2}{m_\rho^2 - 4m_\pi^2} \right)^{\frac{3}{2}}.
 \end{aligned} \tag{5}$$

where m_ρ and Γ_ρ are the $\rho(770)$ mass and width. The transition form factor is parametrized as

$$F_{\rho\eta\gamma}(s) = \sum_V g_V e^{i\phi_V} \frac{m_V^2}{s - m_V^2 + i\sqrt{s}\Gamma_V(s)}, \quad V = \rho(770), \rho(1450), \rho(1700), \tag{6}$$

where $g_V e^{i\phi_V} = g_{V\rho\eta}/g_{V\gamma}$ is the ratio of the coupling constants for the transitions $V \rightarrow \rho\eta$ and $V \rightarrow \gamma^*$.

The data on the visible cross section obtained in this work and in the previous SND measurement in the $\eta \rightarrow \gamma\gamma$ decay mode [1] are fitted simultaneously. The parameters of the $\rho(770)$ resonance are fixed at the current world-average values [18]. The parameter $g_{\rho(770)}$ is calculated using the VMD relation $g_{\rho\rho\eta} = g_{\rho\gamma}g_{\rho\eta\gamma}$ from the $\rho(770) \rightarrow \eta\gamma$ decay width and is equal to $1.59 \pm 0.06 \text{ GeV}^{-1}$. The phase $\phi_\rho(770)$ is set to zero.

Following to Ref. [1] we assume that the coupling constants $g_{V\rho\eta}$ and $g_{V\gamma}$ are real. So the phases $\phi_\rho(1450)$ and $\phi_\rho(1700)$ can take values of 0 or π . The masses, widths, and the constants $g_{\rho(1450)}$ and $g_{\rho(1700)}$ are free fit parameters.

The model with phases $\phi_\rho(1450) = \pi$ and $\phi_\rho(1700) = \pi$ describes data well, $\chi^2/\nu = (37+31)/(39+33-6) = 68/66$, where ν is the number degrees of freedom. The first (second) numbers in the parentheses represent the contribution from the data obtained in this work (Ref. [1]). The values of the radiative correction calculated according to Eq. (3) and the values of the Born cross section obtained using Eq. (1) are listed in Table II. The model uncertainty on the radiative correction is estimated by variation of the model parameters within their errors and is found to be 0.5% below $\sqrt{s} = 1.7 \text{ GeV}$ and 2% above. The systematic uncertainty on the cross section includes the systematic uncertainties on the number of signal events (6%), detection efficiency (see Sec. V), radiative correction, and luminosity (2%). It is equal to 7% below 1.6 GeV and 8% above.

The comparison of the SND measurements in the $\eta \rightarrow 3\pi^0$ and $\eta \rightarrow \gamma\gamma$ decay modes are presented in Fig. 4. Since the data of the two measurements are consistent with each other, we combine them. The combined cross section is listed in the last column of the Table II. For the first six energy points the measurement are done only in the $\eta \rightarrow 3\pi^0$ mode. The systematic uncertainty on the combined cross section is 7% below 1.45 GeV, 6% at $1.45 < \sqrt{s} < 1.6 \text{ GeV}$, and 8% above 1.6 GeV.

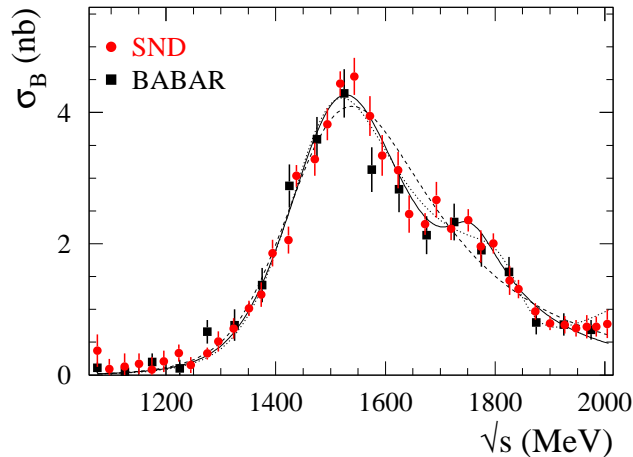


Figure 5: The $e^+e^- \rightarrow \eta\pi^+\pi^-$ Born cross section measured by SND and BABAR [5]. The solid, dashed, and dotted curves are the results of the VMD fit with parameters listed in Table III for Models 1, 2, and 3, respectively.

Table III: Parameters of the VMD model.

Parameter	Model 1	Model 2	Model 3
$g_{\rho(1450)}$ (GeV^{-1})	0.44 ± 0.5	0.56 ± 0.2	0.45 ± 0.3
$\phi_{\rho(1450)}$	π	π	π
$m_{\rho(1450)}$ (MeV/c^2)	1520 ± 10	1510 ± 10	1500 ± 10
$\Gamma_{\rho(1450)}$ (MeV)	320 ± 30	390 ± 10	280 ± 20
$g_{\rho(1700)}$ (GeV^{-1})	$0.024^{+0.019}_{-0.011}$	—	$0.025^{+0.014}_{-0.009}$
$\phi_{\rho(1700)}$	π	—	0
$m_{\rho(1700)}$ (MeV/c^2)	1750 ± 10	—	1840 ± 10
$\Gamma_{\rho(1700)}$ (MeV)	135 ± 50	—	132 ± 40
$g_{\rho(2150)}$ (GeV^{-1})	—	—	0.084 ± 0.008
χ^2/ν	33/33	55/36	29/32

VII. DISCUSSION

The comparison of the combined SND measurement with the previous most precise data obtained by the BABAR Collaboration [5] is presented in Fig. 5. The two data sets are in agreement, but the SND data have better accuracy.

The curves in Fig. 5 represent the results of the fit to the SND data in the three models, which parameters are listed in Table III. In all the models the phase $\phi_{\rho(1450)} = \pi$. The fits with $\phi_{\rho(1450)} = 0$ fail to describe data. Model 1 shown by the solid curve is used in the previous section to calculate the radiative correction. It describes data well, but has a “wrong” value of $\phi_{\rho(1700)}$ equal to π . In the quark model [20] the $e^+e^- \rightarrow \rho(1450) \rightarrow \rho\eta$ and $e^+e^- \rightarrow \rho(1700) \rightarrow \rho\eta$ amplitudes are expected to be opposite in sign. The same prediction for the $e^+e^- \rightarrow \omega\pi$ process is confirmed in Ref. [19]. The fit with the “proper” $\phi_{\rho(1700)} = 0$ gives $g_{\rho(1700)} = 0$ and coincides with Model 2 in Table III. This model shown in Fig. 5 by the dashed curve describes data significantly worse, $P(\chi^2) = 2\%$. It should be noted that in Ref. [1] Model 2 applied to the data obtained in the $\eta \rightarrow \gamma\gamma$ mode gave the reasonable value $P(\chi^2) = 10\%$. So, the addition of the new data obtained in the $\eta \rightarrow 3\pi^0$ mode strongly increases the significance of the $\rho(1700)$ signal.

The reasonable quality of the fit with “proper” $\phi_{\rho(1700)}$ can be obtained in the model with an additional resonance (Model 3 in Table III). The mass and width of this resonance are fixed at the PDG values $m_{\rho(2150)} = 2155 \text{ MeV}/c^2$ and $\Gamma_{\rho(2150)} = 320 \text{ MeV}$. The phase $\phi_{\rho(2150)}$ is set to zero. The result of the fit is shown in Fig. 5 by the dotted curve. More precise data are needed to choose between Models 1 and 3.

The parameters g_V in the fit can be replaced by the products of the branching fractions

$$B(V \rightarrow \rho\eta)B(V \rightarrow e^+e^-) = \frac{\alpha^2 g_V^2 m_V}{9 \Gamma_V^2} P_f(m_V^2). \quad (7)$$

The following values of the products are obtained

$$\begin{aligned} B(\rho(1450) \rightarrow \rho\eta)B(\rho(1450) \rightarrow e^+e^-) \times 10^7 &= (6.9 \pm 0.3)/(7.3 \pm 0.3), \\ B(\rho(1700) \rightarrow \rho\eta)B(\rho(1700) \rightarrow e^+e^-) \times 10^8 &= (4.6_{-1.9}^{+3.0})/(8.3_{-3.1}^{+3.8}) \end{aligned} \quad (8)$$

for Models 1 and 3, respectively. It is interesting that the parameters of the $\rho(1450)$ and $\rho(1700)$ resonances obtained in the two models with different relative phases of the $\rho(1700)$ amplitude are rather close to each other.

VIII. SUMMARY

In this paper the cross section for the process $e^+e^- \rightarrow \eta\pi^+\pi^-$ has been measured in the c.m. energy range from 1.07 to 2.00 GeV in the decay mode $\eta \rightarrow 3\pi^0$. In the range 1.22–2.00 GeV the measured cross section is found to be in good agreement with the previous SND measurement in the $\eta \rightarrow \gamma\gamma$ decay mode [1]. Therefore, the two measurements have been combined.

The cross-section energy dependence has been fitted in the VMD model with 2, 3 and 4 ρ -like states. The quality of the fit with two resonances, $\rho(770)$ and $\rho(1450)$, is quite poor, $P(\chi^2) = 2\%$, while the fits with the additional $\rho(1700)$ resonance describe data well. The $\rho(1700)$ contribution appears as a shoulder on the $\rho(1450)$ peak near 1.75 GeV.

The SND data on the $e^+e^- \rightarrow \eta\pi^+\pi^-$ cross section are in agreement with the previous most precise data obtained by the BABAR Collaboration [5], but have better accuracy.

IX. ACKNOWLEDGMENTS

Part of this work related to the photon reconstruction algorithm in the electromagnetic calorimeter for multiphoton events is supported by the Russian Science Foundation (project No. 14-50-00080).

-
- [1] V. M. Aulchenko *et al.*, Phys. Rev. D **91**, 052013 (2015).
 - [2] V. P. Druzhinin *et al.* (ND Collaboration), Phys. Lett. B **174**, 115 (1986).
 - [3] A. Antonelli *et al.* (DM2 Collaboration), Phys. Lett. B **212**, 133 (1988).
 - [4] R. R. Akhmetshin *et al.* (CMD-2 Collaboration), Phys. Lett. B **489**, 125 (2000).
 - [5] B. Aubert *et al.* (BABAR Collaboration), Phys. Rev. D **76**, 092005 (2007); **77**, 119902(E) (2008).
 - [6] M.N. Achasov *et al.* (SND Collaboration), JETP Lett. **92**, 80 (2010).
 - [7] M.N. Achasov *et al.*, Nucl.Instrum. Methods Phys. Res., Sect. A **598**, 31 (2009); V.M. Aulchenko *et al.*, *ibid.* **598**, 102 (2009); A.Yu. Barnyakov *et al.*, *ibid.* **598**, 163 (2009); V.M. Aulchenko *et al.*, *ibid.* **598**, 340 (2009).
 - [8] A. Romanov *et al.*, in *Proceedings of PAC 2013, Pasadena, CA USA*, p.14.
 - [9] E. V. Abakumova *et al.*, Nucl. Instrum. Meth. A **744**, 35 (2014).
 - [10] E. V. Abakumova, M. N. Achasov, A. A. Krasnov, N. Y. Muchnoi and E. E. Pyata, JINST **10**, T09001 (2015).
 - [11] D. N. Shemyakin *et al.* (CMD-3 Collaboration), Phys. Lett. B **756**, 153 (2016).
 - [12] N. N. Achasov and V. A. Karnakov, JETP Lett. **39** 342 (1984).
 - [13] E. A. Kuraev and V. S. Fadin, Yad. Fiz. **41**, 733 (1985) [Sov. J. Nucl. Phys. **41**, 466 (1985)].
 - [14] G. Bonneau and F. Martin, Nucl. Phys. B **27**, 381 (1971).
 - [15] S. Agostinelli *et al.*, Nucl. Instrum. Methods Phys. Res., Sect. A **506**, **250** (2003).
 - [16] V. P. Druzhinin *et al.*, EPJ Web Conf. **130**, 05004 (2016) [arXiv:1609.01040 [hep-ex]].
 - [17] https://en.wikipedia.org/wiki/ARGUS_distribution
 - [18] K. A. Olive *et al.* (Particle Data Group), Chin. Phys. C, **38**, 090001 (2014).
 - [19] M. N. Achasov *et al.* (SND Collaboration), Phys. Rev. D **94**, 112001 (2016).
 - [20] S. Godfrey and N. Isgur, Phys. Rev. D **32**, 189 (1985).